



**HAL**  
open science

## Characterization of Diblock Copolymers by Capillary Electrophoresis: From Electrophoretic Mobility Distribution to Distribution of Composition

Anthony Phimpachanh, Joseph Chamieh, Laurent Leclercq, Simon Harrisson, Mathias Destarac, Patrick Lacroix-Desmazes, Corine Gerardin, Martin In, Hervé Cottet

### ► To cite this version:

Anthony Phimpachanh, Joseph Chamieh, Laurent Leclercq, Simon Harrisson, Mathias Destarac, et al.. Characterization of Diblock Copolymers by Capillary Electrophoresis: From Electrophoretic Mobility Distribution to Distribution of Composition. *Macromolecules*, 2020, 53 (1), pp.334-345. 10.1021/acs.macromol.9b01978 . hal-02462075v1

**HAL Id: hal-02462075**

**<https://hal.umontpellier.fr/hal-02462075v1>**

Submitted on 2 Dec 2020 (v1), last revised 9 Dec 2020 (v2)

**HAL** is a multi-disciplinary open access archive for the deposit and dissemination of scientific research documents, whether they are published or not. The documents may come from teaching and research institutions in France or abroad, or from public or private research centers.

L'archive ouverte pluridisciplinaire **HAL**, est destinée au dépôt et à la diffusion de documents scientifiques de niveau recherche, publiés ou non, émanant des établissements d'enseignement et de recherche français ou étrangers, des laboratoires publics ou privés.

1 **Characterization of diblock copolymers by capillary electrophoresis: From**  
2 **electrophoretic mobility distribution to distribution of composition**

3 **Anthony Phimpachanh<sup>1,3</sup>, Joseph Chamieh<sup>2</sup>, Laurent Leclercq<sup>2</sup>, Simon Harrisson<sup>4</sup>, Mathias Destarac<sup>4</sup>,**  
4 **Patrick Lacroix-Desmazes<sup>3</sup>, Corine Gérardin<sup>3</sup>, Martin In<sup>1\*</sup>, Hervé Cottet<sup>2\*</sup>**

5 <sup>1</sup>L2C, Univ Montpellier, CNRS, Montpellier, France

6 <sup>2</sup>IBMM, Univ Montpellier, CNRS, ENSCM, Montpellier, France

7 <sup>3</sup>ICGM, Univ Montpellier, CNRS, ENSCM, Montpellier, France

8 <sup>4</sup>IMRCP, University of Toulouse, CNRS UMR5623, Toulouse, France

9 \* Corresponding authors: herve.cottet@umontpellier.fr & martin.in@umontpellier.fr

10 **Abstract**

11 Free solution capillary-electrophoresis (CE) is a powerful separation technique for the  
12 characterization of diblock copolymers. In this work, four series of double-hydrophilic anionic and  
13 cationic block copolymers, namely, poly(acrylamide)-*block*-poly(acrylic acid) (PAM-*b*-PAA),  
14 poly(acrylamide)-*block*- poly((3-acrylamidopropyl)trimethylammonium chloride) (PAM-*b*-PAPTAC),  
15 poly(ethylene oxide)-*block*-poly(acrylic acid) (PEO-*b*-PAA) and poly(poly(ethylene glycol) methyl  
16 ether acrylate)-*block*-poly(acrylic acid) (P(PEGA)-*b*-PAA), were synthesized by reversible addition-  
17 fragmentation chain transfer (RAFT) polymerization and characterized by CE. The electrophoretic  
18 mobility distributions of the copolymers were transformed into distributions of composition ratio by  
19 introducing a retardation parameter,  $X_{exp}$ , that represents the hydrodynamic drag retardation due to the  
20 neutral block of the copolymer. A linear correlation between  $X_{exp}$  and the ratio of the degrees of  
21 polymerization of each blocks was experimentally established and was consistent with the model of  
22 electrophoretic mobility of composite macromolecules with hydrodynamic coupling. Finally, the  
23 comparison of the distributions between the different copolymer families was significantly improved  
24 by considering the distributions in composition ratio compared to the electrophoretic mobility  
25 distributions, since it takes into account the differences in solvation, expansion and drag force  
26 according to the chemical nature of the blocks.

## 27 1 Introduction

28 The characterization of diblock copolymers by separation techniques is challenging but of  
29 primary importance to check their purity and to characterize their distributions in size and in chemical  
30 composition.<sup>1</sup> Block copolymers prepared by reversible deactivation radical polymerization frequently  
31 contain homopolymer impurities.<sup>2, 3</sup> These include dead chains from termination reactions during  
32 polymerization of the first block, as well as the products of side-reactions such as chain transfer to  
33 solvent or monomer during polymerization of the second block. The growth of the second block in  
34 copolymer synthesis is often evidenced by a decrease of the elution time in size-exclusion  
35 chromatography (SEC) as a result of the increased hydrodynamic radius<sup>4, 5</sup>. However, this only holds if  
36 the second block contributes significantly to the hydrodynamic radius of the diblock copolymer.  
37 Getting more quantitative information can be challenging especially in aqueous SEC. Different  
38 solvation properties between the blocks of a block copolymer can lead to coelution of polymers of  
39 different mass in SEC, resulting in inaccuracy in the obtained molar masses.<sup>6</sup> Additionally,  
40 interactions with the stationary phase<sup>3</sup> may lead to HPLC-type elution which is dependent on the  
41 chemical composition of the polymer as well as its size. For diblock copolymer SEC, particular elution  
42 conditions are generally required and size distributions should be expressed in terms of hydrodynamic  
43 radius (and not molar mass) due to the difference in chemical composition / solvation of the two  
44 blocks<sup>6</sup>. The proportion of each monomer in a copolymer can be obtained by liquid chromatography  
45 under critical conditions LCCC, also known as LC-PEAT, for the point of exclusion-adsorption  
46 transition for neutral blocks<sup>7, 8</sup>. The critical conditions for LCCC (or LC-PEAT) are usually difficult to  
47 find and are very sensitive to small changes in mobile phase composition and/or temperature.

48 An alternative separation technique for charged copolymers is free solution capillary  
49 electrophoresis (CE)<sup>2, 3, 7-9</sup>. The electrophoretic separation of charged homopolymers from diblock  
50 copolymers is generally easily obtained in free solution CE. Moreover, for self-assembling diblock  
51 copolymers, CE can also separate micelles from unimers<sup>2, 7, 8</sup> and allows studying the impact of added  
52 surfactant on the copolymer micelles<sup>2, 7</sup>. In the presence of cationic blocks, experimental difficulties

53 arise from polymer adsorption onto the wall of silica based capillaries. The characterization of cationic  
54 diblock copolymers requires the use of a neutrally coated<sup>3</sup>, or positively charged capillary<sup>10</sup>.  
55 Another challenging issue in the characterization of diblock copolymers by CE is to extract the  
56 distribution in composition of the copolymers from the electropherogram. Raw electropherograms can  
57 be transformed into distributions of effective mobility, or of any other related parameter, provided that  
58 the relationship between effective mobility and the considered parameter is known<sup>11</sup>. The  
59 determination of polymer dispersity via the variance of the chemical composition distribution<sup>11</sup> or via  
60 the calculation of the ratio of moments of the distribution has also been studied<sup>1</sup>. A key point to  
61 achieve such electropherogram transformation is to have a reliable relation between the effective  
62 mobility of the diblock copolymer and the degrees of polymerization of each block and thus, to the  
63 chemical composition of the copolymer<sup>3</sup>. The electrophoretic mobility of a diblock copolymer is  
64 generally expressed as a weighted average of the mobilities of different subunits constituting the  
65 copolymer<sup>12</sup>. The choice of the subunits and the corresponding weights have been described in the  
66 literature as depending on the conformations of each block and on the hydrodynamic coupling regime  
67 between the two blocks<sup>12-15</sup>. More recently, Chubynsky and Slater studied in more detail the “end-  
68 effect” (i.e. the fact that the ends of the copolymer chain are more hydrodynamically exposed to the  
69 solvent)<sup>16</sup> and the effect of polymer stiffness on the electrophoretic modeling<sup>17</sup>. The electrophoretic  
70 models of composite objects<sup>12, 13</sup> which are relevant for diblock copolymers, were also applied to end-  
71 labeled free solution electrophoresis (ELFSE)<sup>14, 15</sup>, which consists in attaching a monodisperse neutral  
72 block (drag-tag) to a polydisperse biopolyelectrolyte (for instance, for DNA sequencing in free  
73 solution<sup>15, 18</sup>), or conversely, in attaching a monodisperse polyelectrolyte to a polydisperse neutral  
74 polymer (for instance, for size-based neutral polymer characterization<sup>14</sup>). In this way, the dependence  
75 of electrophoretic mobility with the molar mass of the end-labelled composite object is obtained in  
76 free solution due to the variation of the charge-to-friction ratio.

77 Double-hydrophilic block copolymers (DHBC) are block copolymers containing two  
78 hydrophilic segments. DHBCs on their own are completely soluble in water and do not self-assemble  
79 in dilute conditions. DHBCs can still retain an amphiphilic character and this can lead to self-  
80 organization at the meso-scale in concentrated conditions<sup>19</sup>. They can undergo morphological

81 transitions induced by external stimuli<sup>20</sup> in dilute solution. The great development of reversible  
82 deactivation radical polymerization<sup>21-24</sup> in the last two decades allows tailoring the stimuli-  
83 responsiveness (e.g. to changes in pH, temperature, ionic strength, or light) of these polymers by  
84 controlling both the nature of monomers and the degree of polymerization of the blocks. When one  
85 block is a polyelectrolyte, DHBCs can undergo micellization by electrostatic complexation in the  
86 presence of an oppositely charged polyelectrolyte. These properties lead to a wide range of  
87 applications such as control of crystallization of inorganic compounds<sup>25</sup>, drug delivery<sup>26</sup> or template  
88 for ordered mesoporous materials<sup>27</sup>. For this last application of DHBC, the asymmetry ratio, defined as  
89 the ratio of degrees of polymerization of both blocks, is of crucial interest since it determines the  
90 structure of the DHBC-templated mesoporous materials.

91 It is the aim of the present work to characterize the composition of DHBC by CE, with particular  
92 attention to the asymmetry ratio. The approach has been applied to series of anionic and cationic  
93 DHBCs, namely, poly(acrylamide)-*block*-poly(acrylic acid) (PAM-*b*-PAA), poly(acrylamide)-*block*-  
94 poly((3-acrylamidopropyl)trimethylammonium chloride) (PAM-*b*-PAPTAC), poly(ethylene oxide)-  
95 *block*-poly(acrylic acid) (PEO-*b*-PAA) and poly(poly(ethylene glycol) methyl ether acrylate)-*block*-  
96 poly(acrylic acid) (P(PEGA)-*b*-PAA). These DHBC have been synthesized in aqueous medium by  
97 reversible addition-fragmentation transfer (RAFT) polymerization.

98 In the next section, different models for the electrophoretic mobility of composite objects such as  
99 block copolymers are briefly reviewed. In the third section, the synthesis of the copolymers and the  
100 experimental conditions of their characterization by CE are reported. The results of this work are  
101 presented in section 4, where we describe a method to transform the distribution of electrophoretic  
102 mobility into a distribution of the ratio of degree of polymerization of both blocks.

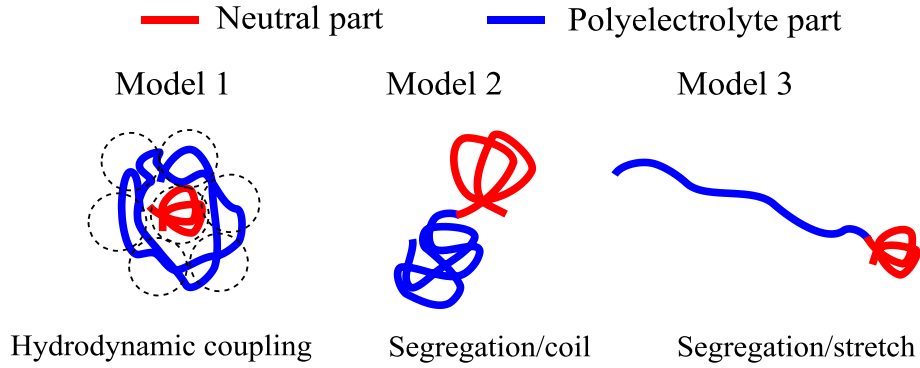


**Figure 1.** Representation of possible conformations of a double hydrophilic block copolymer composed of a neutral Gaussian coil (in red) linked to a polyelectrolyte block (in blue). In model 1, the polyelectrolyte chain is a coil in hydrodynamic interaction with the neutral Gaussian coil. In model 2, the polyelectrolyte and the neutral polymer separate into two coils. In model 3, the polyelectrolyte is fully stretched and has no hydrodynamic coupling with the neutral coil. Adapted from<sup>28</sup>

104 In this section, we present different possible electrophoretic mobility models that are relevant  
 105 for diblock copolymers composed of a polyelectrolyte part attached to a neutral polymer coil. These  
 106 theoretical models were developed by Desruisseaux et al<sup>28</sup>, building on previous work by Long et al.<sup>12</sup>,  
 107 <sup>13</sup> Figure 1 shows the different possible conformations that can be encountered for DHBC,  
 108 corresponding to the different models presented below.

109 **2.1 Model 1: hydrodynamic coupling**

110 In Model 1, hydrodynamic coupling between the polyelectrolyte part and the neutral coil is  
 111 taken into account. The polyelectrolyte block of the DHBC is composed of  $N_{blob}$  equivalent blobs of a  
 112 size equivalent to the hydrodynamic radius of the neutral coil  $R_h^{neutral}$ . If  $R_h^{neutral}$  is larger or equal to  
 113 the Debye length, Long et al.<sup>29</sup> demonstrated that the electrophoretic mobility of the DHBC composite  
 114 object composed of  $N_{blob} + 1$  subunits of equal size, is given by the number-average of the  
 115 electrophoretic mobilities calculated on all the equivalent blobs constituting the object. The  
 116 electrophoretic mobility of the DHBC,  $\mu_{ep,1}^{diblock}$ , is thus given by<sup>28</sup>:

$$\mu_{ep,1}^{diblock} = \frac{\sum_{i=0}^{N_{blob}} \mu_{ep}^i}{N_{blob} + 1} = \frac{N_{blob} \mu_{ep}^0 + \mu_{ep}^{neutral}}{N_{blob} + 1} = \frac{\mu_{ep}^0}{1 + \frac{\alpha}{DP_0}} \quad (1)$$

117 where  $\mu_{ep}^i$  is the effective mobility of the  $i^{\text{th}}$  entity (or blob) constituting the DHBC,  $DP_0$  is the degree  
 118 of polymerization of the polyelectrolyte block,  $\alpha$  is the number of charged monomers per blob,  $\mu_{ep}^0$  is  
 119 the effective electrophoretic mobility of the polyelectrolyte part (alone) and  $\mu_{ep}^{neutral}$  is the  
 120 electrophoretic mobility of the neutral part ( $\mu_{ep}^{neutral} = 0$ ). The number of equivalent blobs in the  
 121 polyelectrolyte chain is given by  $N_{blob} = \frac{DP_0}{\alpha}$ . Note that  $N_{blob}$  (and  $\mu_{ep,1}^{diblock}$ ) depends on the  
 122 polyelectrolyte persistence length, and thus, on the ionic strength. Equation (1) neglects the so-called  
 123 end-effect<sup>16</sup>. Please note that subscript and superscript 0 refer to the polyelectrolyte block, for  
 124 consistency with ref 28.

## 126 2.2 Models without hydrodynamic coupling

### 127 2.2.1 Model 2: polyelectrolyte chain in coil conformation

128 Model 2 in Figure 1 corresponds to the segregation of the neutral polymer coil from the  
 129 polyelectrolyte coil. In the absence of hydrodynamic coupling between the two parts, and if the  
 130 polyelectrolyte chain does not stretch during electrophoresis (i.e. at sufficiently low electric field), the  
 131 electrophoretic mobility of the DHBC,  $\mu_{ep,2}^{diblock}$ , is given by the average electrophoretic mobility of the  
 132 two parts weighted by their hydrodynamic friction coefficient<sup>12</sup>. Using Stokes equation for spherical  
 133 objects,  $\mu_{ep,2}^{diblock}$  is expressed as<sup>13, 28</sup>:

$$\mu_{ep,2}^{diblock} = \frac{\sum_{i=0}^1 \gamma_i \mu_{ep}^i}{\sum_{i=0}^1 \gamma_i} = \frac{\mu_{ep}^0}{1 + \frac{R_h^{neutral}}{R_h^0}} \quad (2)$$

135 where  $\gamma_i$  is the friction coefficient of the  $i^{\text{th}}$  part constituting the DHBC,  $R_h^{\text{neutral}}$  is the hydrodynamic  
 136 radius of the neutral coil,  $R_h^0$  is the hydrodynamic radius of the polyelectrolyte block.

### 137 2.2.2 Model 3: polyelectrolyte chain in fully stretched conformation

138 When the polyelectrolyte coil is stretched under the concomitant influence of the electric field  
 139 and the opposed drag force due to the presence of the neutral coil, it can reach a fully extended  
 140 conformation as depicted in Figure 1 (Model 3). Stokes law is no longer appropriate for the frictional  
 141 coefficient of the polyelectrolyte chain, and the electrophoretic mobility of the DHBC,  $\mu_{ep,3}^{\text{diblock}}$ , is  
 142 given by<sup>27</sup> :

$$143 \mu_{ep,3}^{\text{diblock}} = \frac{\sum_{i=0}^1 \gamma_i \mu_{ep}^i}{\sum_{i=0}^1 \gamma_i} = \frac{\mu_{ep}^0}{1 + \frac{2R_h^{\text{neutral}}}{b_0 DP_0} \ln DP_0} \quad (3)$$

144 where  $b_0$  is the size of a charged monomer in the polyelectrolyte chain. Equation (3) assumes that the  
 145 friction coefficient  $\gamma_{rod}$  of the stretched polyelectrolyte cylinder is averaged on all orientations relative  
 146 to the flow direction, and is given by:

$$147 \gamma_{rod} = \frac{3\pi\eta b_0 DP_0}{\ln(DP_0)} \quad (4)$$

148 where  $\eta$  is the viscosity of the solvent.

149 Even if the electrical field is not strong enough to stretch the polyelectrolyte block (hydrodynamic  
 150 segregation), the polyelectrolyte contour length may still be shorter than the persistence length of the  
 151 polyelectrolyte. In this situation, the segregation between the neutral and the polyelectrolyte parts is  
 152 sterically obtained, but the electrophoretic mobility is still described by equation (3)<sup>27</sup>.



## 153 **3 Experimental**

### 154 **3.1 Chemicals**

155 Ammonium persulfate (APS, 98%) and sodium formaldehyde sulfoxylate dehydrate (NaFS, 98%)  
156 were purchased from Acros organics. Poly(ethylene glycol) methyl ether acrylate ( $M_n = 480$  g/mol, 8.5  
157 EO units on average) and (3-acrylamidopropyl)trimethylammonium chloride (APTAC) aqueous  
158 solution (75 wt.%) were purchased from Sigma Aldrich (Saint-Quentin-Fallavier, France) and used as  
159 received. Acrylic acid from the same suppliers was distilled under vacuum at room temperature. PEO  
160  $M_n=5000$  g.mol<sup>-1</sup>,  $D = 1.04$  was purchased from. 4,4'-azobiscyanopentanoic acid (ACPA, Aldrich,  
161 98%) and 2,2-Azobis(isobutyramidine) dihydrochloride (AIBA, Sigma-Aldrich, 97%) were used as  
162 received.

163  
164 For EC experiments, background electrolytes were prepared in ultra-pure water purified on a Millipore  
165 system (Molsheim, France) from tris(hydroxymethyl)aminomethane (TRIS, 99,9%, Merck), 4-  
166 Morpholinoethanesulphonic acid (MES, >99%, Acros Organics), and 2-[Bis(2-hydroxyethyl)amino]-  
167 2-(hydroxymethyl)propane-1,3-diol (BIS-TRIS, >99%, Acros Organics). Anisic acid (99,5%),  
168 ammediol (99,5%) used as markers for detection were purchased from Sigma-Aldrich.

169

### 170 **3.2 Double-hydrophilic block copolymer synthesis**

171 This section describes the synthesis of the copolymers. The synthetic pathway, the size exclusion  
172 chromatograms and the <sup>1</sup>H NMR spectra are given in SI as well as the temporal electropherograms.

#### 173 **3.2.1 Synthesis of poly(acrylamide)-*b*-poly(acrylic acid)**

##### 174 **Aqueous RAFT/MADIX polymerization of AA**

175 Polyacrylamide macro RAFT/MADIX agent (PAM-Xa,  $M_n = 5000$  g.mol<sup>-1</sup>) was synthesized according  
176 the procedure described by Layrac et al.<sup>30</sup> Synthesis of PAM<sub>70</sub>-*b*-PAA<sub>20</sub> was performed as follows<sup>31</sup>:  
177 PAM-based chain transfer agent (PAM-Xa,) (15.76 g, 3.029 mmol), acrylic acid (4.24 g; 58.77 mmol),  
178 AIBA (0.0821 g, 0,3 mmol) and water (42 g) (solids = 30.6%) were introduced in a round bottom

179 flask. The mixture was degassed with argon at room temperature for 30 min and then placed in a  
180 thermostated oil bath at 65°C under argon for 2 hours. Conversion was quantitative, acrylic acid traces  
181 were eliminated by dialysis (MWCO 1000 Da) and pH-metric monitoring. The polymer solution was  
182 then freeze dried and a white powder was obtained. Four DHBC were synthesized according to this  
183 procedure: PAM<sub>70</sub>-*b*-PAA<sub>20</sub>, PAM<sub>140</sub>-*b*-PAA<sub>40</sub>, PAM<sub>140</sub>-*b*-PAA<sub>60</sub> and PAM<sub>140</sub>-*b*-PAA<sub>80</sub> (see Table 1).

### 184 **3.2.2 Synthesis of poly(acrylamide)-*b*-poly((3-acrylamidopropyl)trimethylammonium** 185 **chloride)**

#### 186 **Aqueous redox RAFT/MADIX polymerization of APTAC**

187 Synthesis of PAM<sub>70</sub>-*b*-PAPTAC<sub>30</sub> was performed as follows: two aqueous solutions of NaFS (5%w)  
188 (1.23 g of solution, 0.4 mmol) and NaPS (5%w) (2.37 mg of solution, 0.5 mmol) were prepared.  
189 PAM-Xa macroxanthate (9.97 g, 1.99 mmol), APTAC monomer (13.3 g of solution, 0.057 mmol), and  
190 water (50 g) (solids = 25.4%) were introduced in a round bottom flask. The pH of the mixture was first  
191 adjusted at 2 with hydrochloric solution 1M. Then the mixture was degassed with argon at room  
192 temperature for 30 min and placed in a thermostated oil bath at 25°C under argon. Both solution of  
193 NaFS and NaPS were introduced in the round bottom flask and the reaction mixture was stirred for 3  
194 hours. Monomer traces were eliminated with dialysis (MWCO 1000 Da) and conductivity monitoring.  
195 The polymer solution was then lyophilized and a white powder was obtained. This redox process at  
196 25°C was developed after the paper of Sutton et al.<sup>9</sup> to minimize the formation of dead chains. Four  
197 DHBC were synthesized according to this procedure: PAM<sub>70</sub>-*b*-PAPTAC<sub>30</sub>, PAM<sub>70</sub>-*b*-PAPTAC<sub>60</sub>,  
198 PAM<sub>140</sub>-*b*-PAPTAC<sub>60</sub> and PAM<sub>140</sub>-*b*-PAPTAC<sub>120</sub> (see Table 1).

### 199 **3.2.3 Synthesis of poly(ethylene oxide)-*b*-poly(acrylic acid)**

#### 200 **Aqueous RAFT polymerization of AA**

201 Synthesis of PEO<sub>105</sub>-*b*-PAA<sub>20</sub> was performed as follows: PEO<sub>105</sub>-CTA (poly(ethylene oxide)-chain  
202 transfer agent) macro RAFT agent was obtained following the procedure published by Bathfield et  
203 al.<sup>32</sup>. PEO<sub>105</sub>-CTA, (10.53 g, 2.19 mmol), ACPA (0.123 mg, 0,439 mmol), acrylic acid (5.5 g, 76  
204 mmol) and deionized water (29.5 mL) (solids=35.4%) were introduced in a Schlenk tube equipped  
205 with a magnetic stirrer. The mixture was degassed by five freeze-evacuate-thaw cycles and then heated

206 for 42 hours at 75°C under nitrogen in a thermostated oil bath. Final conversion = 72%. Monomer  
207 conversion was determined by <sup>1</sup>H NMR spectroscopy, using a Bruker 400MHZ spectrometer. Samples  
208 for analysis by NMR were prepared by adding 0.6 mL of D<sub>2</sub>O to 0.1 mL of polymerization medium.  
209 Once the reaction was complete, the solvent was evaporated, and then the DHBC was dissolved in a  
210 minimum amount of dichloromethane before being precipitated twice in a large volume of cold diethyl  
211 ether. It was then recovered by filtration, and finally dried under vacuum overnight before analysis by  
212 SEC and <sup>1</sup>H-NMR. SEC was performed in DMF-LiBr after methylation<sup>33</sup> with  
213 trimethylsilyldiazomethane. Four DHBC were synthesized according to this procedure: PEO<sub>105</sub>-*b*-  
214 PAA<sub>20</sub>, PEO<sub>105</sub>-*b*-PAA<sub>30</sub>, PEO<sub>210</sub>-*b*-PAA<sub>40</sub> and PEO<sub>210</sub>-*b*-PAA<sub>50</sub> (see Table 1). The degrees of  
215 polymerization of the commercial starting PEO have been determined by <sup>1</sup>H NMR<sup>32</sup> and are presented  
216 in Table 1.

### 217 **3.2.4 Synthesis of poly(acrylic acid)-*b*-poly(poly(ethylene glycol) methyl ether acrylate)**

#### 218 **Aqueous RAFT polymerization of AA and PEGA**

219 5,7-dithia-6-thio-4-methyl-4-cyanodecanoic acid (CTPPA) was obtained by reaction of ACPA  
220 with bis(propylsulfanylthiocarbonyl) disulfide according to literature.<sup>34</sup> Synthesis of PAA<sub>21</sub>-*b*-  
221 P(PEGA)<sub>12</sub> was performed as follows: PAA-CTPPA chain transfer agent was synthesized according to  
222 the process described in literature<sup>35</sup>: in a round bottom flask, CTPPA (0.8 g, 2.57 mmol, purity=89%),  
223 acrylic acid (3.9g, 54.1 mmol), ACPA (0,072 g, 0.26 mmol) and half of the amount of water (7.5 g)  
224 are stirred until dissolution of CTPPA. The remaining water (7.5 g) was introduced and the mixture  
225 was degassed with argon for 40 min. The mixture was then heated in an oil bath at 70°C for 5.5 h. For  
226 the synthesis of PAA-*b*-P(PEGA), ACPA (0.0715 g; 0.26 mmol) and poly(ethylene glycol) methyl  
227 ether acrylate (12.8 g, 26.4 mmol) were added to the PAA-CTPPA reaction medium and the mixture  
228 was degassed with argon for 40 min. The mixture was then heated in an oil bath at 70°C for 5 h.  
229 Conversion was followed by <sup>1</sup>H NMR. At the end of the polymerization, water was evaporated under  
230 reduced pressure and the polymer washed with diethyl ether. NMR sample preparation: 0.6 mL of D<sub>2</sub>O  
231 was added to 0.1 mL of polymerization medium and quenched in liquid nitrogen. Two DHBC were  
232 synthesized according to this procedure: P(PEGA)<sub>12</sub>-*b*-PAA<sub>21</sub> and P(PEGA)<sub>22</sub>-*b*-PAA<sub>45</sub> (see Table 1).

233 **Table 1:** Presentation of the chemical structure and the different DHBC samples synthesized and studied in this  
 234 work. The subscripts in the names correspond to the degree of polymerization of each block.  $MW_{neutral}$  and  $MW_0$   
 235 are the molar masses of the neutral and of the polyelectrolyte block respectively.

| Type of DHBC   | $MW_{neutral}$ - $MW_0$<br>as determined by<br>NMR | Chemical structure |
|--|--|--------------------|
| PAM <sub>70</sub> - <i>b</i> -PAA <sub>20</sub>      | 5k-1.4k  |                    |
| PAM <sub>140</sub> - <i>b</i> -PAA <sub>40</sub>     | 10k-2.8k   |                    |
| PAM <sub>140</sub> - <i>b</i> -PAA <sub>60</sub>     | 10k-4.4k   |                    |
| PAM <sub>140</sub> - <i>b</i> -PAA <sub>80</sub>     | 10k-5.6k   |                    |
| PEO <sub>105</sub> - <i>b</i> -PAA <sub>20</sub>     | 5k-1.4k  |                    |
| PEO <sub>105</sub> - <i>b</i> -PAA <sub>30</sub>     | 5k-2.2k  |                    |
| PEO <sub>210</sub> - <i>b</i> -PAA <sub>40</sub>     | 10k-2.8k   |                    |
| PEO <sub>210</sub> - <i>b</i> -PAA <sub>50</sub>     | 10k-3.6k   |                    |
| PAM <sub>70</sub> - <i>b</i> -PAPTAC <sub>30</sub>   | 5k-5k  |                    |
| PAM <sub>70</sub> - <i>b</i> -PAPTAC <sub>60</sub>   | 5k-10k   |                    |
| PAM <sub>140</sub> - <i>b</i> -PAPTAC <sub>60</sub>  | 10k-10k  |                    |
| PAM <sub>140</sub> - <i>b</i> -PAPTAC <sub>120</sub> | 10k-20k  |                    |
| P(PEGA) <sub>12</sub> - <i>b</i> -PAA <sub>21</sub>  | 5.7k-1.5k  |                    |
| P(PEGA) <sub>22</sub> - <i>b</i> -PAA <sub>45</sub>  | 10.6k-3.2k   |                    |

### 236 3.3 Capillary electrophoresis

#### 237 *Instrumentation and method*

238 Capillary electrophoresis experiments were performed on an Agilent 7100 capillary electrophoresis  
 239 instrument with a diode array UV detector. Fused silica capillaries of 50/375  $\mu\text{m}$  I.D./O.D. with  
 240 polyimide outer coating (cat. no. TSP050375) were from Polymicro Technologies (Phoenix, AZ,

241 USA). Capillary dimensions were 38.5 cm long (30 cm to detection window). New capillaries were  
242 conditioned by performing the following washes at 1 bar: 1M NaOH for 30 min and water for 15 min.  
243 The temperature of the capillary cartridge was set at 25 °C.

244 In the case of PAM-*b*-PAA, an electrolyte consisting of 20 mM MES and 14 mM ammediol pH 6.5  
245 was used. 0.1 g/L anisic acid was added in the sample as a mobility marker. The same background  
246 electrolyte was used for PAM-*b*-PAPTAC, but with a different mobility marker (imidazole 0.1 g/L). In  
247 the case of PEO-*b*-PAA and P(PEGA)-*b*-PAA, an electrolyte constituted of 6 mM anisic acid and 12  
248 mM BIS-TRIS, pH 6.5 was used as buffer, with MES at 0.5 g/L as mobility marker in the case of  
249 P(PEGA)-*b*-PAA.

250 All copolymers were dissolved in water at a concentration of 5 g/L. Samples were injected  
251 hydrodynamically on the inlet side of the capillary by applying 30 mbar for 5 s. Separations were  
252 carried out by applying a +20 kV voltage. For PAM-*b*-PAA, PEO-*b*-PAA and P(PEGA)-*b*-PAA and  
253 PAM-*b*-PAPTAC, detection was realized at 192 +/- 2 nm (reference off).

254 For PAM-*b*-PAA, PEO-*b*-PAA and P(PEGA)-*b*-PAA, the capillary was rinsed between each run by  
255 flushing the capillary for 2 min with the background electrolyte, 2 min with 0.1 M NaOH, 2 min with  
256 ultra-pure water and 2 min with background electrolyte. For the analysis of the cationic polymer  
257 PAM-*b*-PAPTAC, and in order to reduce the adsorption on the capillary wall, surface of the capillary  
258 was modified using UltraTrol™ LN (Target Discovery, Inc., Palo Alto, CA), which is a commercial  
259 neutral semi-permanent coating based on polyacrylamide derivatives. The coating procedure was  
260 performed using the following successive flushes: methanol for 2 min at 1 bar, water for 2 min at  
261 3 bar, 1 M NaOH for 2 min at 3 bar, 0.1 M NaOH for 2 min at 1 bar, 1 M HCl for 5 min at 1 bar, water  
262 for 5 min at 1 bar, UltraTrol™ LN solution for 5 min at 1 bar, wait for 5 min, water for 2 min at 1 bar.  
263 Prior to each analysis of PAM-*b*-PAPTAC, the capillary was rinsed with the background electrolyte  
264 for 2 min at 1 bar.

265

266 **Electropherogram data treatment**

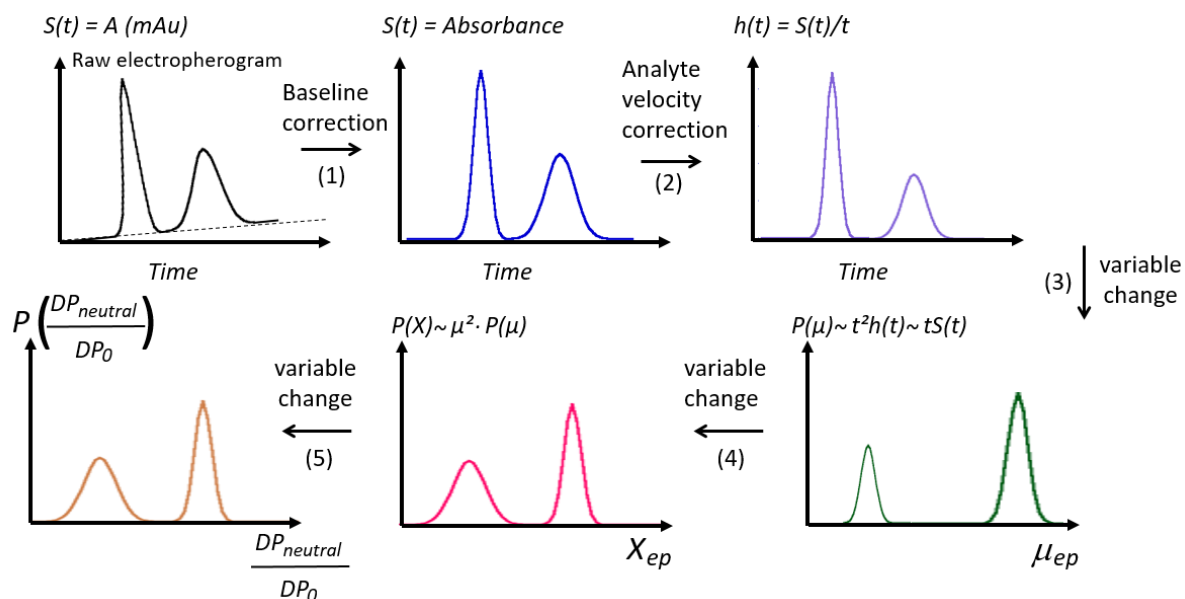


**Figure 2.** General scheme for changing a time-scale electropherogram into a mobility-scale and  $X_{\text{exp}}$ -scale distributions. The raw electropherogram is first corrected from baseline shift (1). The time-scale electropherogram is then corrected from the differences in analyte velocities (2). The time-corrected electropherogram is converted into the effective mobility-scale distribution (3). The mobility-scale electropherogram is changed into a  $X_{\text{exp}}$ -scale distribution (4) and finally to a compositional  $\frac{DP_{\text{neutral}}}{DP_0}$  ratio (5).

$S(t)$  is the UV absorbance signal (in mAU).  $h(t)$  is the time-corrected UV absorbance.  $P(\mu_{\text{ep}})$  is the effective mobility distribution.  $P(X_{\text{exp}})$  is the distribution in  $X_{\text{exp}}$  (see section 4.2) and  $P(\frac{DP_{\text{neutral}}}{DP_0})$  is the distribution in  $\frac{DP_{\text{neutral}}}{DP_0}$ .

$\frac{DP_{\text{neutral}}}{DP_0}$ . Adapted from<sup>11</sup> for the characterization of diblock copolymers.

267 **Scale transformations.** In this section, the transformations of the electropherograms into distributions  
 268 of the parameter of interest are described following a previously published protocol<sup>11</sup>. Briefly,  
 269 experimental raw time-scale electropherograms, were first corrected from any baseline shift using  
 270 Origin (Origin 2016, OriginLab, USA) as depicted in step 1, Figure 2. For quantitative purpose, the  
 271 absorbance signal  $S(t)$  was next divided by the migration time ( $t$ ) to correct the differences in analyte

272 velocity (Figure 2, step 2)<sup>11</sup>. Next, the time-corrected electropherogram  $h(t)$  was changed into an  
 273 effective mobility distribution  $P(\mu_{ep}) = t \times S(t)$  (Figure 2, step 3)<sup>11</sup>, which requires the  
 274 transformations of both the  $x$  and  $y$  axis<sup>11</sup>. Note that  $\mu_{ep}$  is obtained by equation (5):

$$275 \quad \mu_{ep} = \frac{lL}{V} \left( \frac{1}{t} - \frac{1}{t_{eo}} \right) \quad (5)$$

276 where  $l$  is the effective capillary length,  $L$  is the total capillary length,  $t$  is the migration time,  $t_{eo}$  is the  
 277 EOF marker migration time and  $V$  is the separation voltage.

278 **Moments of the electrophoretic mobility distribution** The average effective mobility of the diblock  
 279 copolymer  $\overline{\mu_{ep}^{diblock}}$  was obtained by integration of the peak of the copolymer in the effective mobility  
 280 scale according to:

$$281 \quad \overline{\mu_{ep}^{diblock}} = \frac{\int P(\mu_{ep}) \mu_{ep} d\mu_{ep}}{\int P(\mu_{ep}) d\mu_{ep}} \approx \frac{\sum_i P(\mu_{ep,i}) \mu_{ep,i} (\mu_{ep,i+1} - \mu_{ep,i})}{\sum_i P(\mu_{ep,i}) (\mu_{ep,i+1} - \mu_{ep,i})} \quad (6)$$

282 where integration is carried out over the peak. In practice the integration is done numerically and the  $i$   
 283 index represents the digitized experimental data points. The summation is carried out over values of  
 284  $P(\mu_{ep,i})$  greater than the median of the base line added to its standard deviation. Calculation of  
 285  $\overline{\mu_{ep}^{diblock}}$  was performed using Excel 2016 (Microsoft, USA), following the discrete form of equation  
 286 (6). Variance of the diblock electrophoretic mobility was obtained by the following equation:

$$287 \quad \sigma_{\mu}^2 = \frac{\int P(\mu_{ep}) \left( \mu_{ep} - \overline{\mu_{ep}^{diblock}} \right)^2 d\mu_{ep}}{\int P(\mu_{ep}) d\mu_{ep}} = \frac{\sum_i P(\mu_{ep,i}) (\mu_{ep,i} - \overline{\mu_{ep}^{diblock}})^2 (\mu_{ep,i+1} - \mu_{ep,i})}{\sum_i P(\mu_{ep,i}) (\mu_{ep,i+1} - \mu_{ep,i})} \quad (7)$$

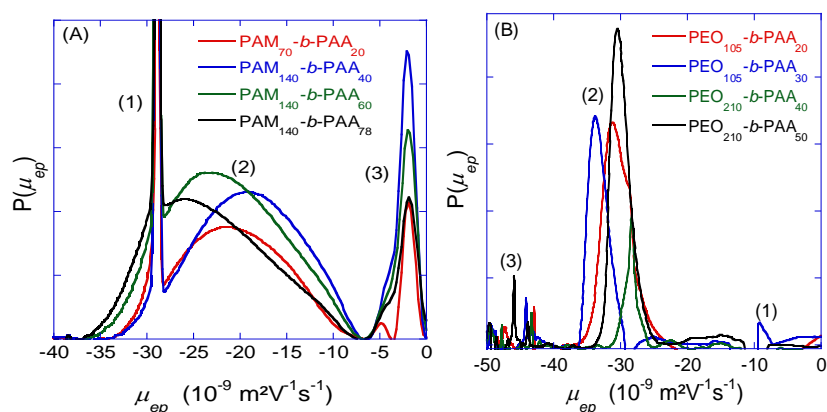
288

## 289 4. Results and discussion

### 290 4.1. Electrophoretic separation of the DHBC

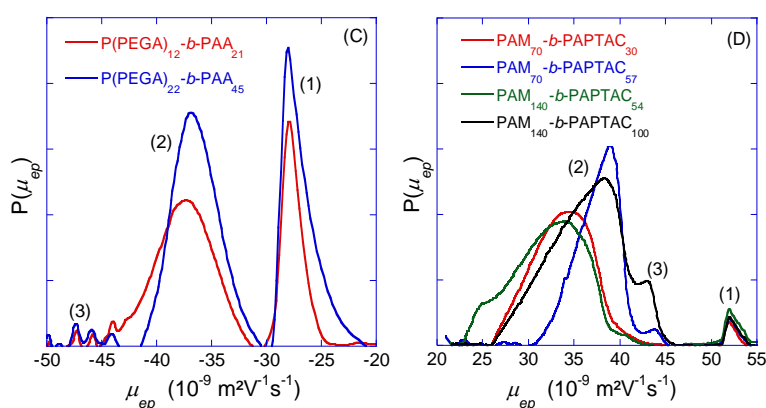
291 The main goal of the CE characterization is to provide information about the chemical composition  
292 distribution of the DHBC and about the purity of the DHBC in terms of possible presence of  
293 homopolymers. The separation of the DHBC by CE requires an appropriate background electrolyte,  
294 depending on the nature of the copolymer. For copolymers absorbing in UV (i.e. those with a PAM  
295 neutral block), direct UV detection was possible and a background electrolyte based on 20 mM MES  
296 and 14 mM ammonium dihydrogen phosphate at pH 6.5 was used, with a UV detection at 192 nm. For DHBC copolymers that  
297 do not absorb UV enough to ensure sensitivity (i.e. PEO-*b*-PAA or P(PEGA)-*b*-PAA), an indirect  
298 detection mode based on a 6 mM anisic acid and 12 mM BIS TRIS at pH 6.5 was used. At this pH  
299 about 60% of the carboxylic acid groups of the PAA are ionized, and this ensures appropriate  
300 selectivity of separation between PAA homopolyelectrolyte and the DHBC. Uncoated fused silica  
301 capillary was used for the characterization of all anionic DHBC. Semi-permanent UltraTrollLN neutral  
302 coating was used for the characterization of the cationic PAM-*b*-PAPTAC DHBC, to avoid any  
303 copolymer adsorption on the capillary surface. To correct the apparent mobility from the  
304 electroosmotic mobility, a mobility marker (anisic acid for PAM-*b*-PAA, MES for P(PEGA)-*b*-PAA,  
305 and imidazolium for PAM-*b*-PAPTAC) of known effective mobility ( $\mu_{ep, MES} = -28$  TU (where TU,  
306 Tiselius Unit, stands for  $10^{-9} \text{ m}^2\text{V}^{-1}\text{s}^{-1}$ ) and  $\mu_{ep, imidazolium} = 52$  TU) was co-injected. For PEO-*b*-PAA, the  
307 electroosmotic mobility was estimated from the electroosmotic flow (EOF) peak. The distributions of  
308 effective mobility (DEM) of PAM-*b*-PAA, PEO-*b*-PAA, P(PEGA)-*b*-PAA and PAM-*b*-PAPTAC are  
309 displayed in Figure 3.





310

311



312

313 **Figure 3.:** Distributions of effective electrophoretic mobility obtained for PAM-*b*-PAA (A), PEO-*b*-  
 314 PAA (B), P(PEGA)-*b*-PAA (C), and PAM-*b*-PAPTAC (D).-Electrophoretic conditions: fused silica  
 315 capillary (A, B, C) or coated with UltraTrolLN<sup>TM</sup> (D), 50  $\mu\text{m}$  I.D.  $\times$  38.5 cm (effective length, 30 cm).  
 316 Electrolytes: 20 mM MES, 14 mM ammediol, pH 6.5 (A, D); 6 mM anisic acid, 12 mM BIS TRIS, pH  
 317 6.5 (B, C). Applied voltage: +20 kV. Hydrodynamic injection: 30 mbar, 5 s. Direct (A, D) or indirect  
 318 (B, C) UV detection at 192 $\pm$  2 nm. Temperature: 25  $^{\circ}\text{C}$ . Samples: 5 g/L DHBC. Assignment of the  
 319 peaks: PAM-*b*-PAA (A): anisic acid (1), DHBC (2), PAM homopolymer (3); PEO-*b*-PAA (B): system  
 320 peak (1), DHBC (2), PAA oligomers (3); P(PEGA)-*b*-PAA (C): MES (1), DHBC (2), PAA oligomers  
 321 (3); PAM-*b*-PAPTAC (D): Imidazolium (1), DHBC (2), PAPTAC (3). The degree of polymerization  
 322 of each block is specified on the graph.

323 The DEM in the series PAM-*b*-PAA (Figure 3A) show three peaks, two sharp at -29 TU (peak 1) and  
 324 -2 TU (peak 3) and one broad (peak 2) between -7 and -37.5 TU, the latter being assigned to the

325 copolymer of interest. The peak at -29 TU is assigned to anisic acid (electrophoretic mobility marker)  
326 and the one at -2 TU corresponds to homopolymer of PAM. The non-zero electrophoretic mobility of  
327 the PAM homopolymer is explained by the incorporation of the negatively charged initiator 4,4'-  
328 azobis(4-cyanopentanoic) acid. The mass proportion of this PAM population of dead chains has been  
329 quantified by external calibration based on time-corrected peak areas using direct injections of PAM  
330 solutions of known concentration in the same condition as the DHBC. The proportion of PAM  
331 homopolymer amounts to 21wt% in the solid form polymer sample for PAM<sub>70</sub>-*b*-PAA<sub>20</sub>, 15% for  
332 PAM<sub>140</sub>-*b*-PAA<sub>40</sub> and PAM<sub>140</sub>-*b*-PAA<sub>60</sub> and 8% for PAM<sub>140</sub>-*b*-PAA<sub>78</sub>. The copolymer peak is broad  
333 and, as expected, the DEM shifts further from zero as the proportion of charged monomer increases in  
334 the composition of the copolymers. This can be verified by comparing the average electrophoretic  
335 mobility value  $\overline{\mu_{ep}^{diblock}}$  (given in Table 2) which varies between -19.5 TU and -24.1 TU from PAM<sub>140</sub>-  
336 *b*-PAA<sub>40</sub> to PAM<sub>140</sub>-*b*-PAA<sub>78</sub>. The greater the average molar mass of the polymer, the more dispersed  
337 its electrophoretic mobility, as demonstrated by the standard deviation  $\sigma_{\mu}$  which varies from 3.9 TU  
338 for PAM-*b*-PAA 70-20, to 6.2 TU for PAM-*b*-PAA 140-60.

339 The DEM of PEO based copolymers are presented in Figure 3B for linear PEO and Figure 3C for PEO  
340 grafted polyacrylates (P(PEGA)). Three populations are observed in both series: several small peaks  
341 associated with large electrophoretic mobility at -45TU are assigned to short oligomers of PAA, the  
342 weight percent of which is estimated to be lower than 10%. The sensitivity of the UV detection is too  
343 low to conclude about the presence / absence of PEO or P(PEGA) in the DHBC. The least mobile  
344 species at -28TU in Figure 3C corresponds to the MES used as mobility marker. The peak at  
345 intermediate values of mobility corresponds to the DHBC. The electrophoretic mobility of PEO-*b*-  
346 PAA ( $\overline{\mu_{ep}^{diblock}}$  ranging from -28 to -33 TU, Table 2) is significantly closer to zero than that of  
347 P(PEGA)-*b*-PAA copolymers ( $\overline{\mu_{ep}^{diblock}}$  ranging from -36 to -38 TU, Table 2), although the molar  
348 masses are close. This is because P(PEGA), a comb-like polymer, is more compact than linear PEO of  
349 the same molar mass. As a consequence, the drag force due to the neutral block is lower for P(PEGA)  
350 than for PEO.

351 As for PAM-*b*-PAPTAC copolymer, PAPTAC homopolymer was detected at about +43TU, as a  
352 shoulder merged in the copolymer distribution, only for the  $DP_{neutral}/DP_0$  equal to 140/100 and 70/57  
353 samples. Figure 3D displays DEM ranged between +22 and +41 TU, with higher effective mobilities  
354 for the DHBC of highest charge. Comparison of PAM-*b*-PAA series with PAM-*b*-PAPTAC series  
355 illustrates the importance of the nature of the blocks on the drag effect of the neutral block. This effect  
356 is discussed in more detail in section 4.2.

357 As a general trend, electrophoretic mobilities of DHBC are always closer to zero than those of the  
358 homopolyelectrolyte which are:  $\mu_{PAA} = -42$  TU;  $\mu_{PAPTAC} = +44$  TU, and the electrophoretic mobility of  
359 the DHBC increases as the proportion of charged monomers in the DHBC increases (see Figure SI  
360 20). In terms of EM dispersion, the least dispersed series is the P(PEGA)-*b*-PAA, with relative  
361 standard deviation of EM  $\sigma_{\mu} / \overline{\mu_{ep}^{diblock}}$  between 6.5% to 9%, followed by the PEO-*b*-PAA (  
362  $\sigma_{\mu} / \overline{\mu_{ep}^{diblock}} \sim 5\%$  to 16%) and the most disperse series is the PAM-*b*-PAA series with 20% to 30%  
363 relative standard deviation of the electrophoretic mobility. This dispersion in mobility results from  
364 both the level of control of the polymerization, and from the spatial extension of the polymer in the  
365 solvent. It can be explained by the chemistry of the RAFT polymerization (chain transfer agent R-  
366 SC(S)Z where Z is the activating group and R is the leaving group), for which the polymerization of  
367 acrylates is better controlled by dithiobenzoates (Z: -SC(S)Ph) ( $\mathfrak{D} < 1.2$ ) than by ethyl xanthate (Z: -  
368 SC(S)OEt) ( $\mathfrak{D} > 1.3$ ). Besides, the 2-phenylacetate ester of PEO is a better homolytic leaving group  
369 than PAM.<sup>36</sup> Furthermore, the synthesis of PAM-*b*-PAA cumulates two successive RAFT/MADIX  
370 polymerizations of AM and AA, whereas the synthesis of PEO-*b*-PAA starts from a narrow PEO-CTA  
371 ( $\mathfrak{D} = 1.04$ ) (PEO obtained by anionic polymerization) to perform a single RAFT polymerization of  
372 AA. This is consistent with the higher dispersity of PAM-*b*-PAA compared to PEO-*b*-PAA<sup>31</sup>. In  
373 addition, in reversible-deactivation radical polymerization<sup>37</sup>, at full conversion, the dispersity as  
374 defined by the ratio of the weight average molar mass over the number average molar mass, decreases  
375 when the  $DP$  increases<sup>38</sup>:

$$D = 1 + \frac{1}{DP} + \frac{1}{C_{ex}} \quad (8)$$

where  $DP$  is the targeted polymerization degree and  $C_{ex}$  is the degenerative chain transfer constant between dormant and active chains<sup>39, 40</sup>, which is consistent with a higher dispersity for a shorter poly(acrylic acid) block in PEO-*b*-PAA.

To get a better description of the copolymer distribution, it would be interesting to get a distribution of a new parameter which is directly related to the chemical composition of the copolymer instead of the electrophoretic mobility, which is not linearly dependent on the copolymer composition. This is the purpose of the two following sections.

384

|                             | $DP_{neutral}$<br>$DP_0$ | $\mu_{ep}^{diblock}$<br>peak<br>max<br>(TU) | $\overline{\mu_{ep}^{diblock}}$<br>integration<br>(TU) | $\sigma_{\mu}$<br>(TU) | $X_{exp}$<br>peak<br>max | $\overline{X_{exp}}$ by<br>integration | $\sigma_{X_{exp}}$ |
|-----------------------------|--------------------------|---|--|------------------------|--------------------------|--|--------------------|
| <b>PAM-<i>b</i>-PAA</b>     | 70-20                    | -22   | -19.9  | 3.89                   | 0.61                     | 1.12                                   | 0.45               |
|                             | 140-40                   | -19.1                                       | -19.5  | 5.44                   | 0.74                     | 1.26                                   | 0.73               |
|                             | 140-60                   | -23.3                                       | -21.4  | 6.19                   | 0.58                     | 1.05                                   | 1.0                |
|                             | 140-78                   | -25.3                                       | -24.1  | 5.68                   | 0.41                     | 0.99                                   | 0.56               |
| <b>PEO-<i>b</i>-PAA</b>     | 105-20                   | -31   | -30.2  | 4.83                   | 0.28                     | 0.33                                   | 0.12               |
|                             | 105-30                   | -33.8                                       | -33.2  | 2.45                   | 0.18                     | 0.21                                   | 0.06               |
|                             | 210-40                   | -28   | -28.4  | 1.36                   | 0.40                     | 0.41                                   | 0.06               |
|                             | 210-50                   | -30.5                                       | -30  | 1.97                   | 0.30                     | 0.34                                   | 0.64               |
| <b>P(PEGA)-<i>b</i>-PAA</b> | 21-11.5                  | -37.6                                       | -38.6  | 3.61                   | 0.059                    | 0.043                                  | 0.09               |
|                             | 44.9-22.2                | -37   | -36.6  | 2.41                   | 0.079                    | 0.098                                  | 0.08               |

|         |      |      |      |      |       |      |
|---------|------|------|------|------|-------|------|
| 70-30   | 34.6 | 33.9 | 3.18 | 0.19 | 0.25  | 0.12 |
| 70-60   | 39.1 | 37.1 | 3.2  | 0.08 | 0.11  | 0.05 |
| 140-60  | 34.2 | 32   | 4.1  | 0.21 | 0.32  | 0.39 |
| 140-120 | 38.5 | 36.3 | 4.1  | 0.09 | 0.164 | 0.13 |

385 **Table 2.** Electrophoretic mobility  $\mu_{ep}^{diblock}$  at peak maximum and average value  $\overline{\mu_{ep}^{diblock}}$  obtained by peak  
386 integration, standard deviation of the electrophoretic mobility distribution  $\sigma_{\mu}$ ,  $X_{exp}$  value at peak maximum and  
387 average value  $\overline{X_{exp}}$  obtained by peak integration, standard deviation of the  $X_{exp}$  distribution  $\sigma_{X_{exp}}$  of all DHBC  
388 studied in this work. Note that the peak of anisic acid was first subtracted before integration for the calculation of  
389  $\overline{\mu_{ep}^{diblock}}$  and  $\sigma_{\mu}$  for PAM-*b*-PAA.

390

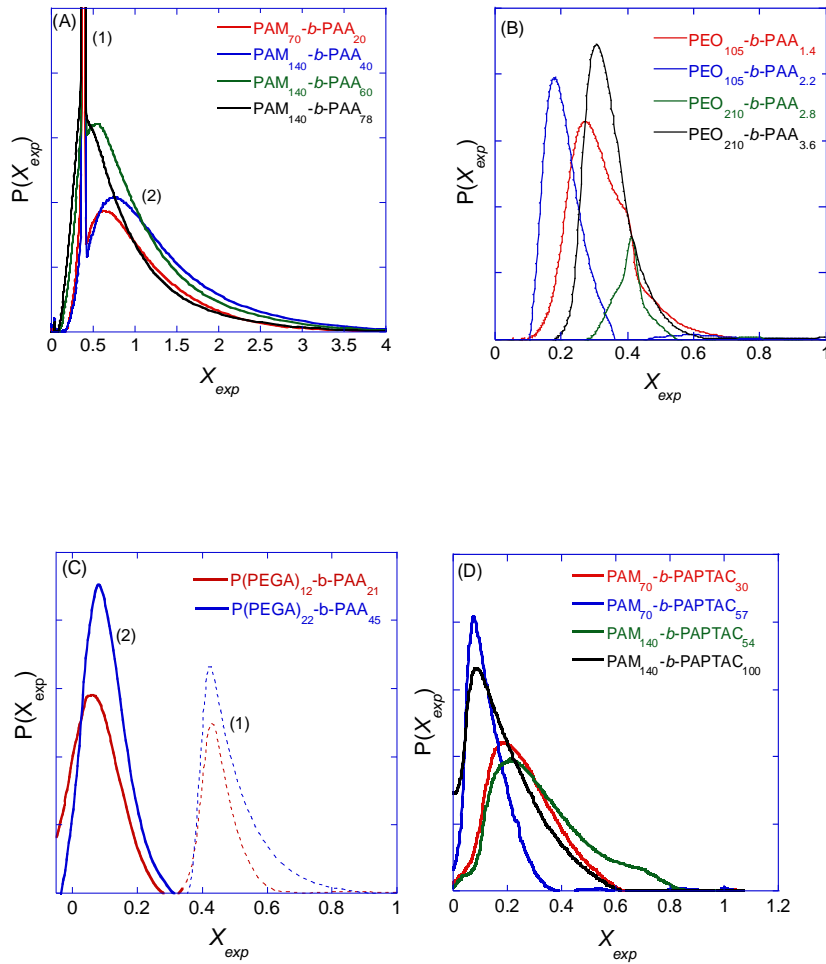
#### 391 4.2. Change of variable from $\mu_{ep}$ to the retardation parameter $X_{exp}$

392 The drag effect of the neutral block can be expressed by the retardation parameter  $X_{exp}$  defined as :

$$393 \quad X_{exp} = \frac{\mu_{ep}^0 - \mu_{ep}^{diblock}}{\mu_{ep}^{diblock}} = \frac{\mu_{ep}^0}{\mu_{ep}^{diblock}} - 1 \quad (9)$$

394 where  $\mu_{ep}^0$  is the electrophoretic mobility of the homopolyelectrolyte;  $\mu_{ep}^{diblock}$  is the electrophoretic  
395 mobility of the copolymer.  $X_{exp}$  expresses the relative decrease of mobility due to the presence of the  
396 neutral block. It is positive and increases as the drag effect increases.

397



398

399

400

401 **Figure 4.** Distribution of retardation parameter  $X_{exp}$  for PAM-*b*-PAA (A) PEO-*b*-PAA (B), P(PEGA)-  
 402 *b*-PAA (C), and PAM-*b*-PAPTAC (D). Experimental conditions as in Figure 3  $X_{exp}$  was determined  
 403 using eq. (8), eq. (12) and  $\mu_{ep,PAA}^0 = -42TU$ ;  $\mu_{ep,PAPTAC}^0 = 44 TU$ . Assignment of the peaks: PAM-*b*-  
 404 PAA (A): anisic acid (1), DHBC (2); P(PEGA)-*b*-PAA (C): MES (1), DHBC (2). The degree of  
 405 polymerization of each block is specified on the graph.

406

407 The new experimental variable,  $X_{exp}$ , not only points out the friction due to the neutral block but is also  
 408 more directly related to the composition of the DHBC. Introducing equation (9) in the various  
 409 expressions of the electrophoretic mobility (equations 1 to 3),  $X_{exp}$ , can be expressed as a function of

410 the ratio between the degrees of polymerization of the neutral  $DP_{neutral}$  and the charged blocks  $DP_0$ .

411 Taking into account the hydrodynamic coupling (model 1),  $X_{exp}$  reads:

$$412 \quad X_{model,1} = \frac{1}{N_{blob}} = \frac{\alpha}{DP_0} \quad (10a)$$

413 and can be further developed as a function of the Kuhn lengths of the neutral block,  $b_{K_1}$ , and of the

414 polyelectrolyte,  $b_{K_0}$ :<sup>15, 41</sup>

$$415 \quad X_{model,1} = \alpha_1 \frac{DP_{neutral}}{DP_0} \quad (10b)$$

$$416 \quad \text{with } \alpha_1 = \frac{b_1 b_{K_1}}{b_0 b_{K_0}} \quad (10c)$$

417 where  $b_1$  is the neutral monomer size. The Kuhn statistical segment length (which is twice the  
418 persistence length) is a measure of the polymer stiffness. Parameter  $\alpha_1$  in Equation (10b) is a relative  
419 friction coefficient and it is non-dimensional. Since the polyelectrolyte is generally stiffer than the  
420 neutral block,  $\alpha_1$  is often much smaller than unity<sup>15</sup>.

421 As for model 2, it is clear from equation (2) that the  $X$  parameter is directly expressed as the ratio of  
422 the hydrodynamic radius of each block:

$$423 \quad X_{model,2} = \frac{R_h^{neutral}}{R_h^0} \quad (11a)$$

424 which can be rewritten as a function of the degrees of polymerization of each block by:

$$425 \quad X_{model,2} = \frac{C_1 DP_{neutral}^{a_1}}{C_0 DP_0^{a_0}} \quad (11b)$$

426 where  $C_1$  (resp.  $C_2$ ) and  $a_1$  (resp.  $a_2$ ) are, respectively, the prefactors and exponents for the neutral  
427 (resp. charged) block in the relationship between  $R_h$  and  $DP$ . Note that  $a_0$  and  $a_1$  are supposed to be  
428 close to 0.5-0.6 for coil conformations, and slightly higher for more extended conformations.

429 As for model 3 (see equation (3)), the  $X$  parameter is directly expressed as:

$$430 \quad X_{\text{model},3} = \frac{2R_h^{\text{neutral}} \ln DP_0}{b_0 DP_0} \quad (12a)$$

431 Injecting  $R_h^{\text{neutral}}$  in equation (9a) leads to:

$$432 \quad X_{\text{model},3} = \frac{2C_1 DP_{\text{neutral}}^{a_1} \ln DP_0}{b_0 DP_0} \quad (12b)$$

433 Finally, equations (10b) (11b) and (12b) demonstrates that, whatever the considered model, the  $X$   
 434 parameter is related to a compositional ratio between the neutral and the charged blocks with,  
 435 however, different scaling dependences with the  $DP$  of each block, and with an additional logarithmic  
 436 term in model 3. It is worth noting that in the case of hydrodynamic coupling (model 1), the newly  
 437 introduced variable varies linearly with the ratio of degree of polymerization of the two blocks.

438 The distributions of the  $X_{\text{exp}}$  parameter are simply deduced from the distribution of electrophoretic  
 439 mobility using the following equation (Figure 2, step 4)<sup>11</sup>:

$$440 \quad P(X_{\text{exp}}) = \left| \frac{1}{\frac{\partial X_{\text{ep}}}{\partial \mu_{\text{ep}}}} \right| P(\mu_{\text{ep}}) = \mu_{\text{ep}}^2 P(\mu_{\text{ep}}) \quad (13)$$

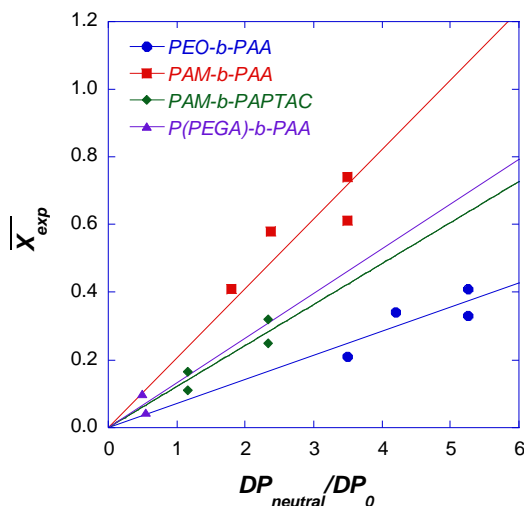
441 All the  $X_{\text{exp}}$  distributions are presented in Figure 4. Since  $\mu_{\text{ep}}$  and  $X_{\text{exp}}$  are not linearly related, the  
 442 change of the variable from  $\mu_{\text{ep}}$  to  $X_{\text{exp}}$  modify the form of the distribution. The different moments  
 443 characterizing the distribution of  $X_{\text{exp}}$  are calculated using similar relations as equations (6) and (7) and  
 444 are reported in Table 2.

445  $X_{\text{exp}}$  range varies between 0.1-3 for PAM-*b*-PAA, 0.1-0.7 for PEO-*b*-PAA, 0-0.3 for P(PEGA)-*b*-PAA  
 446 and 0-0.8 for PAM-*b*-PAPTAC. The dispersion of the retardation parameter  $X_{\text{exp}}$  expressed as  $\sigma_{X_{\text{exp}}}$   
 447 values (Table 2) follows the following order: P(PEGA)-*b*-PAA < PEO-*b*-PAA ~ PAM-*b*-PAPTAC <  
 448 PAM-*b*-PAA. The dispersion of the retardation parameter cannot be interpreted as a dispersity in



449 molar mass or in composition since the retardation parameter will change with these chemical features  
 450 in a way that depends on the conformation of the blocks. So, a further step is needed to get the  
 451 composition dispersion.

452 **4.3. Change of variable from  $X_{exp}$  to chemical composition ratio**



453  
 454 **Figure 5.** Plot of  $\overline{X}_{exp}$  against  $\frac{DP_{neutral}}{DP_0}$ .  $\overline{X}_{exp}$  was determined by using eq.(6) after replacing  $\mu_{ep}$  by  
 455  $X_{exp} \cdot \frac{DP_{neutral}}{DP_0}$  was obtained by NMR (see Table 1). Least-square linear regressions provide the following  
 456 experimental slopes: 0.071+/-0.005 for PEO-b-PAA; 0.12+/-0.01 for PAM-b-PAPTAC; 0.13 +/- 0.01  
 457 for P(PEGA)-b-PAA; 0.21+/-0.02 for PAM-b-PAA.

458  
 459 To go further in the interpretation and in the process of the experimental data, it is crucial to identify  
 460 the model which is best adapted to describe the electrophoretic behavior of the DHBC investigated in  
 461 this work. To assess the validity of model 1 (hydrodynamic coupling between blocks, see section 2.3),  
 462  $\overline{X}_{exp}$  was plotted against  $\frac{DP_{neutral}}{DP_0}$  in Figure 5 for the four DHBC families.

463 **Table 3.** Characteristic parameters of neutral and charged blocks constituting the DHBC studied in this work.  
 464  $M_w$  are expressed in g/mol.

|        | $b_l$ (nm)          | $b_{k_1}$ (nm)     | $R_h^{neutral}$ (nm) <sup>a</sup>          | 465 |
|--------|---------------------|--------------------|--|-----|
| PAM    | 0.25                | 0.6 <sup>42</sup>  | $0.01447 \times M_w^{0.57}$ <sup>43</sup>  | 466 |
| PEO    | 0.3 <sup>44</sup>   | 0.74 <sup>44</sup> | $0.02398 \times M_w^{0.53}$ <sup>45</sup>  | 467 |
|        | $b_0$ (nm)          | $b_{k_0}$ (nm)     | $R_h^0$ (nm)                               | 468 |
| PAA    | 0.25                | 2.5 <sup>46</sup>  | $0.007906 \times M_w^{0.585}$ <sup>2</sup> | 469 |
| PAPTAC | approximated as PAA |                    |  | 470 |

471

472 <sup>a</sup> From Mark-Houwink parameters using  $R_h = \left( \frac{3[\eta]M}{10\pi N_A} \right)^{1/3}$ , where  $[\eta]$  is the intrinsic viscosity and  $N_A$  is  
473 the Avogadro number. from ref<sup>46</sup> (see Table 1 and Figure 13(a) herein).

474

475 The results are consistent with model 1 which predicts a linear dependence of the retardation  
476 parameter  $\overline{X_{exp}}$  on the ratio of degree of polymerization  $\frac{DP_{neutral}}{DP_0}$ . The slopes determined from the  
477 graph in Figure 5 correspond to the parameter  $\alpha_1$  in equation (10b) which can be calculated from  
478 equation (10c). Experimentally, the numerical values of the slopes  $\alpha_{1,exp}$  are in the range of ~0.1-0.2.  
479 Taking the characteristic parameters (Kuhn lengths, monomer dimensions) given in Table 3 leads to  
480  $\alpha_1=0.24$  (vs  $\alpha_{1,exp}=0.21\pm 0.02$  experimentally obtained) for PAM-*b*-PAA,  $\alpha_1=0.36$  (vs  $\alpha_{1,exp}=0.071\pm$   
481  $0.005$ ) for PEO-*b*-PAA, and  $\alpha_1=0.24$  (vs  $\alpha_{1,exp}=0.12\pm 0.01$ ) for PAM-*b*-PAPTAC. Theoretical values  
482 of  $\alpha_1$  are in a reasonably good agreement with the experimental ones, knowing the uncertainty on the  
483 persistence length (notably for the polyelectrolyte blocks) and monomer sizes. As for P(PEGA)-*b*-  
484 PAA, we only get an estimation of  $\alpha_{1,exp}=0.13$ , since the P(PEGA) Kuhn length is not available in the  
485 literature. From Figure 5, we can conclude that the linear correlation between  $\overline{X_{exp}}$  and  $\frac{DP_{neutral}}{DP_0}$  is  
486 confirmed and that model 1 (with hydrodynamic coupling between the two blocks) can be used to

487 transform the  $X_{\text{exp}}$  distributions into compositional  $\frac{DP_{\text{neutral}}}{DP_0}$  distributions. As for models 2 and 3, they

488 lead to poor correlations between theoretical  $X_{\text{model},i}$  versus experimental  $\overline{X_{\text{exp}}}$  values (see Figure 6).

489 The knowledge of  $\alpha_i$  provides the last relation necessary to carry on the general scheme presented in  
490 Figure 2 to its end and which leads to the distribution of ratio of chemical composition. In practice, we  
491 used  $\alpha_{i,\text{exp}}$  obtained in Figure 5 together with equation (10b) to transform the data of Figures 4A to 4D  
492 into the distributions presented in Figures 7A to 7D, using the following equation:

$$493 \quad P\left(\frac{DP_{\text{neutral}}}{DP_0}\right) = \frac{P(X)}{\frac{\partial\left(\frac{DP_{\text{neutral}}}{DP_0}\right)}{\partial X}} = \alpha_1 P(X) \quad (14)$$

494 Since  $X_{\text{exp}}$  and  $\frac{DP_{\text{neutral}}}{DP_0}$  are linearly correlated, the shapes of both distributions are similar. However,

495 reading  $\frac{DP_{\text{neutral}}}{DP_0}$  axis, which corresponds to a compositional ratio, is more convenient for the

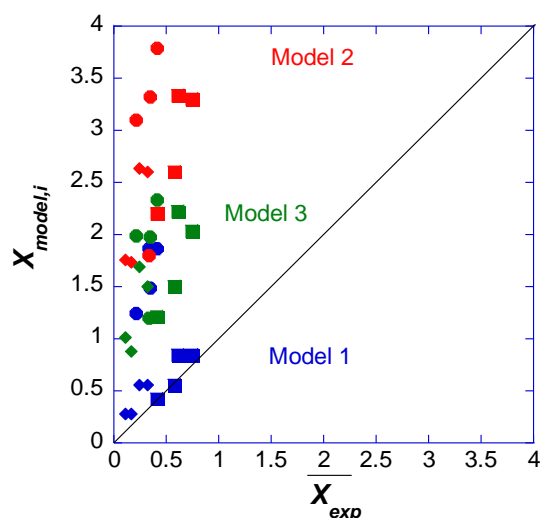
496 practitioners than keeping the  $X_{\text{exp}}$  scale. Moreover, and as previously anticipated, since the  $\alpha_i$

497 coefficients are different from one DHBC to another, the distribution in  $\frac{DP_{\text{neutral}}}{DP_0}$  allows a better

498 comparison between them. On the whole, the dispersion of the composition ratio are in the order of:

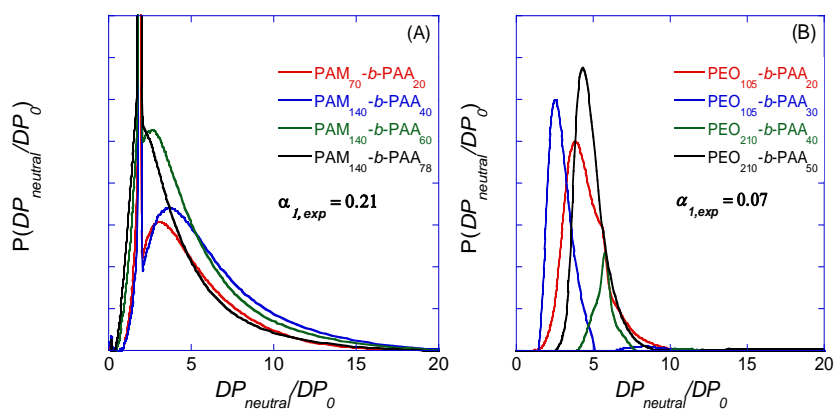
499 P(PEGA)-*b*-PAA < PAM-*b*-PAPTAC ~ PEO-*b*-PAA < PAM-*b*-PAA.

500

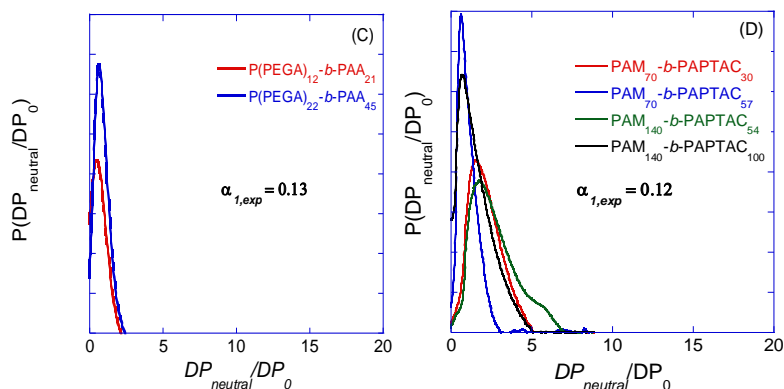


501  
 502 **Figure 6.** Comparison between  $X_{model,i}$  and  $\overline{X}_{exp}$  for the three different models using theoretical  
 503 parameters given in Table 3. PAM-*b*-PAPTAC (◆); PEO-*b*-PAA (●); PAM-*b*-PAA (■).  $\overline{X}_{exp}$  was  
 504 determined by integration of the DHBC peak (in *X* scale). For all  $X_{model,i}$  calculations, theoretical  
 505  $DP_{neutral}$  and  $DP_0$  were used.  $X_{model,1}$  was determined according to equations (10b) and (10c),  $X_{model,2}$   
 506 according to equation (11a) and  $X_{model,3}$  according to equations (12a), with the characteristic  
 507 numerical parameters given in Table 3.

508



509



510

511 **Figure 7.** Distribution of composition in terms of the ratio of the degrees of polymerization of both  
 512 blocks for PAM-*b*-PAA (A), PEO-*b*-PAA (B), P(PEGA)-*b*-PAA (C), and PAM-*b*-PAPTAC (D).

513 Experimental conditions as in Figure 3.  $\frac{DP_{neutral}}{DP_0}$  was determined using eq. (10b) and  $P\left(\frac{DP_{neutral}}{DP_0}\right)$  was

514 obtained using eq. (14). In (C), the MES peak has been removed. In (A), the sharp peak is a mobility  
 515 marker (anisic acid) and was deleted before peak integration.

516

## 517 Conclusion

518 In an effort to make information provided by capillary electrophoresis more directly useful for  
 519 polymer chemists, a protocol was proposed to convert electrophoretic mobility distributions of double  
 520 hydrophilic block copolymers into distributions of chemical composition ratios. This ratio of  
 521 composition is expressed as the ratio of the degrees of polymerization of each block  $\frac{DP_{neutral}}{DP_0}$ . To get

522 this composition ratio, we have introduced the retardation parameter  $X$  which takes into account the  
 523 drag force exerted by the neutral block on the polyelectrolyte. The distribution of  $X$  that characterizes a  
 524 DHBC is readily obtained from the experimental electropherogram and the relation between  $X$  and the  
 525 ratio of  $DP$ . The latter is available from different models for electrophoretic mobility of composite  
 526 objects. A linear relation has been found experimentally between the retardation parameter  $X$  and the  
 527 ratio of  $DP$ s, within each of the four families of DHBC studied in this work. This result is consistent  
 528 with the model of electrophoretic mobility of Long *et al.* that takes into account hydrodynamic

529 coupling, although the prefactors are slightly overestimated. Our experimental findings not only  
530 support the theoretical prediction, but also facilitate the last step of data transformation, from  
531 distribution of  $X$  into distributions of ratios of  $DP$ .

532 The dispersions in composition are in the order of: P(PEGA)-*b*-PAA < PEO-*b*-PAA ~ PAM-*b*-  
533 PAPTAC < PAM-*b*-PAA. Therefore, we can conclude that in the DHBC families, the PAM block  
534 leads to broader composition ratio distributions compared to a PEO block, when associated to a PAA  
535 block. Similarly, the P(PEGA) block lead to less disperse composition ratio distributions compared to  
536 a PEO block, when associated to a PAA block. Finally, PAA associated with PAM leads to broader  
537 composition ratio distributions compared to PAPTAC associated with PAM. The relatively low  
538 composition dispersity of the PEO-PAA block copolymer is most likely due to the low dispersity of  
539 the PEO block, prepared by anionic polymerization, and the use of a dithiobenzoate chain transfer  
540 agent, which has a higher chain transfer constant and thus gives narrower molar mass distributions  
541 than the xanthate chain transfer agent used to prepare the PAM-PAA and PAM-PAPTAC block  
542 copolymers. The use of a trithiocarbonate chain transfer agent and a relatively short P(PEGA) block  
543 leads to a fairly narrow composition distribution for P(PEGA)-PAA block copolymers.

544 Finally, the transformation of electrophoretic mobility distributions into composition ratio  
545 distributions significantly improved the comparison of the distributions between the different  
546 copolymer families, since it takes into account the differences in expansion and drag force according  
547 to the chemical nature of the blocks.

#### 548 **Supporting Information.**

549 Synthetic pathway, SEC and NMR characterizations, raw electropherograms are provided for all  
550 dibloc copolymers studied in this work.

551 **Acknowledgements**

552 This work was supported by the MESOPIC project funded by the Agence Nationale de la Recherche  
553 (ANR) under grant # ANR-15-CE07-0005.

554 **References**

- 555 1. Thevarajah, J. J.; Sutton, A. T.; Maniego, A. R.; Whitty, E. G.; Harrison, S.; Cottet, H.;  
556 Castignolles, P.; Gaborieau, M., Quantifying the Heterogeneity of Chemical Structures in Complex  
557 Charged Polymers through the Dispersity of Their Distributions of Electrophoretic Mobilities or of  
558 Compositions. *Anal. Chem.* **2016**, *88* (3), 1674-1681.
- 559 2. Morel, A.; Cottet, H.; In, M.; Deroo, S.; Destarac, M., Electrophoretic Behavior of  
560 Amphiphilic Diblock Copolymer Micelles. *Macromolecules* **2005**, *38* (15), 6620-6628.
- 561 3. Sutton, A. T.; Read, E.; Maniego, A. R.; Thevarajah, J. J.; Marty, J. D.; Destarac, M.;  
562 Gaborieau, M.; Castignolles, P., Purity of Double Hydrophilic Block Copolymers Revealed by Capillary  
563 Electrophoresis in the Critical Conditions. *J. Chromatogr. A* **2014**, *1372C*, 187-195.
- 564 4. Javakhishvili, I.; Jankova, K.; Hvilsted, S., Neutral, Anionic, Cationic, and Zwitterionic Diblock  
565 Copolymers Featuring Poly(2-methoxyethyl acrylate)“Hydrophobic” Segments. *Polym. Chem.-UK*  
566 **2013**, *4* (3), 662-668.
- 567 5. Delplace, V.; Harrison, S.; Tardy, A.; Gimes, D.; Guillaneuf, Y.; Nicolas, J.,  
568 Nitroxide-Mediated Radical Ring-Opening Copolymerization: Chain-End Investigation and Block  
569 Copolymer Synthesis. *Macromol. Rapid Comm.* **2014**, *35* (4), 484-491.
- 570 6. Nejad, E. H.; Castignolles, P.; Gilbert, R. G.; Guillaneuf, Y., Synthesis of Methacrylate  
571 Derivatives Oligomers by Dithiobenzoate-RAFT-Mediated Polymerization. *J. Polym. Sci. A1* **2008**, *46*  
572 (6), 2277-2289.
- 573 7. Jacquin, M.; Muller, P.; Cottet, H.; Crooks, R.; Théodoly, O., Controlling the Melting of  
574 Kinetically Frozen Poly(butyl acrylate-*b*-acrylic acid) Micelles via Addition of Surfactant. *Langmuir*  
575 **2007**, *23* (20), 9939-9948.

- 576 8. Jacquin, M.; Muller, P.; Lizarraga, G.; Bauer, C.; Cottet, H.; Théodoly, O., Characterization of  
577 Amphiphilic Diblock Copolymers Synthesized by MADIX Polymerization Process. *Macromolecules*  
578 **2007**, *40* (8), 2672-2682.
- 579 9. Jacquin, M.; Muller, P.; Cottet, H.; Théodoly, O., Self-Assembly of Charged Amphiphilic  
580 Diblock Copolymers with Insoluble Blocks of Decreasing Hydrophobicity: From Kinetically Frozen  
581 Colloids to Macrosurfactants. *Langmuir* **2010**, *26* (24), 18681-18693.
- 582 10. Anik, N.; Airiau, M.; Labeau, M.-P.; Vuong, C.-T.; Reboul, J.; Lacroix-Desmazes, P.;  
583 Gérardin, C.; Cottet, H., Determination of Polymer Effective Charge by Indirect UV Detection in  
584 Capillary Electrophoresis: Toward the Characterization of Macromolecular Architectures.  
585 *Macromolecules* **2009**, *42* (7), 2767-2774.
- 586 11. Chamieh, J.; Martin, M.; Cottet, H., Quantitative Analysis in Capillary Electrophoresis:  
587 Transformation of Raw Electropherograms Into Continuous Distributions. *Anal. Chem.* **2015**, *87* (2),  
588 1050-1057.
- 589 12. Long, D.; Ajdari, A., Electrophoretic Mobility of Composite Objects in Free Solution:  
590 Application to DNA Separation. *Electrophoresis* **1996**, *17* (6), 1161-1166.
- 591 13. Long, D.; Viovy, J.-L.; Ajdari, A., Simultaneous Action of Electric Fields and Nonelectric Forces  
592 on a Polyelectrolyte: Motion and Deformation. *Phys. Rev. Lett.* **1996**, *76* (20), 3858-3861.
- 593 14. Vreeland, W. N.; Desruisseaux, C.; Karger, A. E.; Drouin, G.; Slater, G. W.; Barron, A. E.,  
594 Molar Mass Profiling of Synthetic Polymers by Free-Solution Capillary Electrophoresis of DNA-  
595 Polymer Conjugates. *Anal. Chem.* **2001**, *73* (8), 1795-1803.
- 596 15. Nedelcu, S.; Slater, G. W., Branched Polymeric Labels Used as Drag-Tags in Free-Solution  
597 Electrophoresis of ssDNA. *Electrophoresis* **2005**, *26* (21), 4003-4015.
- 598 16. Chubynsky, M. V.; Slater, G. W., Theory of End-Labeled Free-Solution Electrophoresis: Is the  
599 End Effect Important? *Electrophoresis* **2014**, *35* (5), 596-604.
- 600 17. Chubynsky, M. V.; Slater, G. W., Electrophoresis of Heteropolymers. Effect of Stiffness.  
601 *Macromolecules* **2015**, *48* (16), 5899-5913.



- 602 18. Desruisseaux, C.; Long, D.; Drouin, G.; Slater, G. W., Electrophoresis of Composite Molecular  
603 Objects. 1. Relation between Friction, Charge, and Ionic Strength in Free Solution. *Macromolecules*  
604 **2001**, *34* (1), 44-52.
- 605 19. Schmidt, B. V. K. J., Double Hydrophilic Block Copolymer Self-Assembly in Aqueous Solution.  
606 *Macromol. Chem. Phys.* **2018**, *219* (7), 1700494.
- 607 20. Guragain, S.; Bastakoti, B. P.; Malgras, V.; Nakashima, K.; Yamauchi, Y., Multi-Stimuli-  
608 Responsive Polymeric Materials. *Chem-Eur. J.* **2015**, *21* (38), 13164-74.
- 609 21. Perrier, S., 50th Anniversary Perspective: RAFT Polymerization—A User Guide.  
610 *Macromolecules* **2017**, *50* (19), 7433-7447.
- 611 22. Matyjaszewski K., X. J., Atom Transfer Radical Polymerization. *Chem. Rev.* **2001**, *100*, 2921-  
612 2990.
- 613 23. Nicolas, J.; Guillaeneuf, Y.; Lefay, C.; Bertin, D.; Gigmes, D.; Charleux, B., Nitroxide-Mediated  
614 Polymerization. *Prog. Polym. Sci.* **2013**, *38* (1), 63-235.
- 615 24. Destarac, M., Industrial Development of Reversible-Deactivation Radical Polymerization: is  
616 the Induction Period Over? *Polym. Chem.-UK* **2018**, *9* (40), 4947-4967.
- 617 25. Colfen, H., Double-Hydrophilic Block Copolymers: Synthesis and Application as Novel  
618 Surfactants and Crystal Growth Modifiers. *Macromol. Rapid Comm.* **2001**, *22*, 219-252.
- 619 26. Loh, X. J.; del Barrio, J.; Toh, P. P. C.; Lee, T.-C.; Jiao, D.; Rauwald, U.; Appel, E. A.;  
620 Scherman, O. A., Triply Triggered Doxorubicin Release From Supramolecular Nanocontainers.  
621 *Biomacromolecules* **2012**, *13* (1), 84-91.
- 622 27. Baccile, N.; Reboul, J.; Blanc, B.; Coq, B.; Lacroix-Desmazes, P.; In, M.; Gerardin, C.,  
623 Ecodesign of Ordered Mesoporous Materials Obtained with Switchable Micellar Assemblies. *Angew.*  
624 *Chem. Int. Edit.* **2008**, *47*, 8433-8437.
- 625 28. Desruisseaux, C.; Drouin, G.; Slater, G. W., Electrophoresis of Composite Molecular Objects.  
626 2. Competition between Sieving and Frictional Effects in Polymer Solutions. *Macromolecules* **2001**, *34*  
627 (15), 5280-5286.

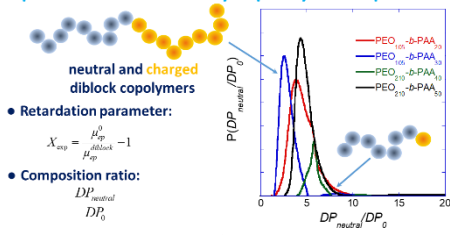
- 628 29. Long, D.; Dobrynin, A. V.; Rubinstein, M.; Ajdari, A., Electrophoresis of polyampholytes. *The*  
629 *J. Chem. Phys.* **1998**, *108* (3), 1234-1244.
- 630 30. Layrac, G.; Gérardin, C.; Tichit, D.; Harrisson, S.; Destarac, M., Hybrid Polyion Complex  
631 Micelles from Poly(Vinylphosphonic Acid)-Based Double Hydrophilic Block Copolymers and Divalent  
632 Transition Metal Ions. *Polymer* **2015**, *72*, 292-300.
- 633 31. Taton, D.; Wilczewska, A.-Z.; Destarac, M., Direct Synthesis of Double Hydrophilic Statistical  
634 Di- and Triblock Copolymers Comprised of Acrylamide and Acrylic Acid Units via the MADIX Process.  
635 *Macromol. Rapid Comm.* **2001**, *22* (18).
- 636 32. Bathfield, M.; Warnant, J.; Gérardin, C.; Lacroix-Desmazes, P., Asymmetric Neutral, Cationic  
637 and Anionic PEO-Based Double-Hydrophilic Block Copolymers (DHBCs): Synthesis and Reversible  
638 Micellization Triggered by Temperature or pH. *Polym. Chem.-UK* **2015**, *6* (8), 1339-1349.
- 639 33. Kuhnel, E.; Laffan, D. D.; Lloyd-Jones, G. C.; Martinez Del Campo, T.; Shepperson, I. R.;  
640 Slaughter, J. L., Mechanism of Methyl Esterification of Carboxylic Acids by  
641 Trimethylsilyldiazomethane. *Angew. Chem. Int. Edit* **2007**, *46* (37), 7075-8.
- 642 34. Boursier, T.; Chaduc, I.; Rieger, J.; D'Agosto, F.; Lansalot, M.; Charleux, B., Controlled  
643 Radical Polymerization of Styrene in Miniemulsion Mediated by PEO-based Trithiocarbonate  
644 Macromolecular RAFT Agents. *Polym. Chem.-UK* **2011**, *2* (2), 355-362.
- 645 35. Chaduc, I.; Crepet, A.; Boyron, O.; Charleux, B.; D'Agosto, F.; Lansalot, M., Effect of the pH  
646 on the RAFT Polymerization of Acrylic Acid in Water. Application to the Synthesis of Poly(acrylic acid)-  
647 Stabilized Polystyrene Particles by RAFT Emulsion Polymerization. *Macromolecules* **2013**, *46* (15),  
648 6013-6023.
- 649 36. Moad, G.; Rizzardo, E.; Thang, S. H., Living Radical Polymerization by the RAFT Process ? A  
650 Third Update. *Aust. J. of Chem.* **2012**, *65* (8), 985.
- 651 37. Jenkins, A. D.; Jones, R. G.; Moad, G., Terminology for Reversible-Deactivation Radical  
652 Polymerization Previously Called "Controlled" Radical or "Living" Radical Polymerization (IUPAC  
653 Recommendations 2010). *Pure Appl. Chem.* **2009**, *82* (2).

- 654 38. Harrisson, S., The Downside of Dispersity: Why the Standard Deviation is a Better Measure of  
655 Dispersion in Precision Polymerization. *Polym. Chem.-UK* **2018**, *9* (12), 1366-1370.
- 656 39. Goto, A.; Fukuda, T., Kinetics of Living Radical Polymerization. *Prog. Polym. Sci.* **2004**, *29* (4),  
657 329-385.
- 658 40. Molina, E.; Warnant, J.; Mathonnat, M.; Bathfield, M.; In, M.; Laurencin, D.; Jerome, C.;  
659 Lacroix-Desmazes, P.; Marcotte, N.; Gerardin, C., Drug-Polymer Electrostatic Complexes as New  
660 Structuring Agents for the Formation of Drug-Loaded Ordered Mesoporous Silica. *Langmuir* **2015**, *31*  
661 (47), 12839-12844.
- 662 41. McCormick, L.; Slater, G.; Karger, A.; Vreeland, W.; Barron, A.; Desruisseaux, C.; Drouin, G.,  
663 Capillary Electrophoretic Separation of Uncharged Polymers Using Polyelectrolyte Engines:  
664 Theoretical Model. *J. Chromatogr. A* **2001**, *924* (1-2), 43-52.
- 665 42. Zhang, W.; Zou, S.; Wang, C.; Zhang, X., Single Polymer Chain Elongation of Poly(N-  
666 isopropylacrylamide) and Poly(acrylamide) by Atomic Force Microscopy. *J. Phys. Chem. B* **2000**, *104*  
667 (44), 10258-10264.
- 668 43. J. Brandrup, E. H. I., E. A. Grulke *Polymer Handbook, Fourth Edition, Vol. 2.* John Wiley and  
669 Sons, Hoboken, New Jersey ed.; 1999; Vol. 2.
- 670 44. Lee, H.; Venable, R. M.; MacKerell, A. D.; Pastor, R. W., Molecular Dynamics Studies of  
671 Polyethylene Oxide and Polyethylene Glycol: Hydrodynamic Radius and Shape Anisotropy. *Biophys. J.*  
672 **2008**, *95* (4), 1590-1599.
- 673 45. Armstrong, J. K.; Wenby, R. B.; Meiselman, H. J.; Fisher, T. C., The Hydrodynamic Radii of  
674 Macromolecules and Their Effect on Red Blood Cell Aggregation. *Biophys. J.* **2004**, *87* (6), 4259-4270.
- 675 46. Cranford, S. W.; Buehler, M. J., Variation of Weak Polyelectrolyte Persistence Length through  
676 an Electrostatic Contour Length. *Macromolecules* **2012**, *45* (19), 8067-8082.

677

678 **For TOC only:**

### Composition distributions by Capillary Electrophoresis



679

680